# Neural excitability and sensory input determine intensity perception with opposing directions in initial cortical responses

Stephani, T.[1, 2]*, Hodapp, A.[1¶], Jamshidi Idaji, M.[1, 2, 3], Villringer, A.[1, 4, 5], Nikulin, V. V.[1, 6]*

[1] Department of Neurology, Max Planck Institute for Human Cognitive and Brain Sciences, Leipzig, Germany, 04103

[2] International Max Planck Research School NeuroCom, Leipzig, Germany, 04103

[3] Machine Learning Group, Technical University of Berlin, Berlin, Germany, 10587

[4] Berlin School of Mind and Brain, Humboldt-Universität zu Berlin, Berlin, Germany, 10117

[5] Clinic for Cognitive Neurology, University Hospital Leipzig, Leipzig, Germany, 04103

[6] Institute for Cognitive Neuroscience, National Research University Higher School of Economics, Moscow, Russian Federation, 101000

[¶] Now at Department of Psychology, University of Potsdam, Potsdam, Germany, 14476

* corresponding authors: T.S. (stephani@cbs.mpg.de); V.V.N. (nikulin@cbs.mpg.de)

# 1   Abstract

2       Perception of sensory information is determined by stimulus features (e.g., intensity)

3   and instantaneous neural states (e.g., excitability). Commonly, it is assumed that both are

4   reflected similarly in evoked brain potentials, that is, higher evoked activity leads to a

5   stronger percept of a stimulus. We tested this assumption in a somatosensory discrimination

6   task in humans, simultaneously assessing (i) single-trial excitatory post-synaptic currents

7   inferred from short-latency somatosensory evoked potentials (SEP), (ii) pre-stimulus alpha

8   oscillations (8-13 Hz), and (iii) peripheral nerve measures. Fluctuations of neural excitability

9   shaped the perceived stimulus intensity already during the very first cortical response (at

10   ~20 ms) yet demonstrating opposite neural signatures as compared to the effect of presented

11   stimulus intensity. We reconcile this discrepancy via a common framework based on

12   modulations of electro-chemical membrane gradients linking neural states and responses,

13   which calls for reconsidering conventional interpretations of brain potential magnitudes in

14   stimulus intensity encoding.

# 1    Introduction

15

16        Even for the very same stimulus, the brain´s response differs from moment to moment.

17    This has been explained by ever-changing neural states (Arieli et al., 1996), with behaviorally

18    relevant consequences (Waschke et al., 2021). Specifically, these changes of neural states are

19    often conceptualized as fluctuations of cortical excitability (Jensen & Mazaheri, 2010;

20    Klimesch et al., 2007; Romei et al., 2008). In the human brain, a commonly hypothesized

21    marker of cortical excitability is oscillatory activity in the alpha band (8-13 Hz), which can be

22    measured with electro- and magnetoencephalography (EEG/MEG). This marker has been

23    associated with modulations of a stimulus´ percept in various sensory domains including the

24    visual (Busch et al., 2009; Iemi et al., 2017), auditory (Müller et al., 2013), and

25    somatosensory domain (Baumgarten et al., 2016; Craddock et al., 2017; Forschack et al.,

26    2020). According to the baseline sensory excitability model (BSEM; Samaha et al., 2020),

27    higher alpha activity preceding a stimulus leads to a generally lower excitability level of the

28    neural system, resulting in a lower detection rate of near-threshold stimuli but no changes in

29    the discriminability of sensory stimuli. On a cellular level, such excitability modulations may

30    be reflected in changes of membrane potentials (Castro-Alamancos, 2009), which may occur

31    in an oscillatory manner (Lakatos et al., 2005) and shift the threshold for incoming sensory

32    information to be processed further downstream in the neural system. This notion has been

33    further supported by monkey studies showing that higher oscillatory activity within the alpha

34    band is associated with a lower neural firing rate (Bollimunta et al., 2011; Haegens et al.,

35    2011).

36        However, it remains unclear up to now whether the influence of instantaneous

37    excitability on perceptual processes can be generalized to the intensity perception of stimuli

38    *per se* (i.e., beyond the sensory threshold) – which would have far-reaching implications for a

39    wide variety of studies in the field of perception. Moreover, if such modulation indeed occurs,

40    the question remains: At which stage of the neural response cascade do instantaneous

41  excitability changes begin to interact with the sensory input in order to shape the brain´s

42  response in a behaviorally relevant way?

43      A unique opportunity to non-invasively measure instantaneous excitability changes of

44  neurons involved in the first cortical response to sensory stimuli in humans is offered by the

45  N20 component of the somatosensory evoked potential (SEP) as measured with EEG: The

46  N20 component, a negative deflection after around 20 ms at centro-parietal electrode sites in

47  response to median nerve stimulation, reflects excitatory post-synaptic potentials (EPSPs) of

48  the first thalamo-cortical volley (Bruyns-Haylett et al., 2017; Nicholson Peterson et al., 1995;

49  Wikström et al., 1996) which are generated in the anterior wall of the postcentral gyrus,

50  Brodmann area 3b (Allison et al., 1991). When keeping the sensory input constant, the

51  amplitude of this early part of the SEP thus represents a direct measure of the instantaneous

52  excitability of a well-defined neuronal population in the primary somatosensory cortex.

53  Notably, amplitude fluctuations of the N20 component have recently been found to relate to

54  pre-stimulus alpha activity both at a given instance as well as through their long-term

55  temporal dynamics, which suggests that both measures reflect a common modulating factor,

56  that is cortical excitability (Stephani et al., 2020).

57      In the current study, we set out to examine the implications of instantaneous

58  excitability fluctuations at initial cortical processing – as measured both by pre-stimulus alpha

59  activity and N20 amplitudes – on the perceived intensity of somatosensory stimuli. We used a

60  binary intensity rating task in which participants were to discriminate supra-threshold median

61  nerve stimuli of two intensities in a continuous stimulation sequence (Fig. 1a). Our results

62  show that both pre-stimulus alpha activity and N20 amplitudes are associated with a bias in

63  the perceived intensity of somatosensory stimuli. Thus, instantaneous excitability fluctuations

64  affect sensory brain responses already at earliest possible cortical processing with

65  behaviorally relevant consequences. Counterintuitively, elevated neural excitability and

66  stronger stimulus intensity resulted in reverse effects on short-latency SEP amplitudes, which

4

67    in turn may offer further insights into the neural mechanisms of excitability regulation

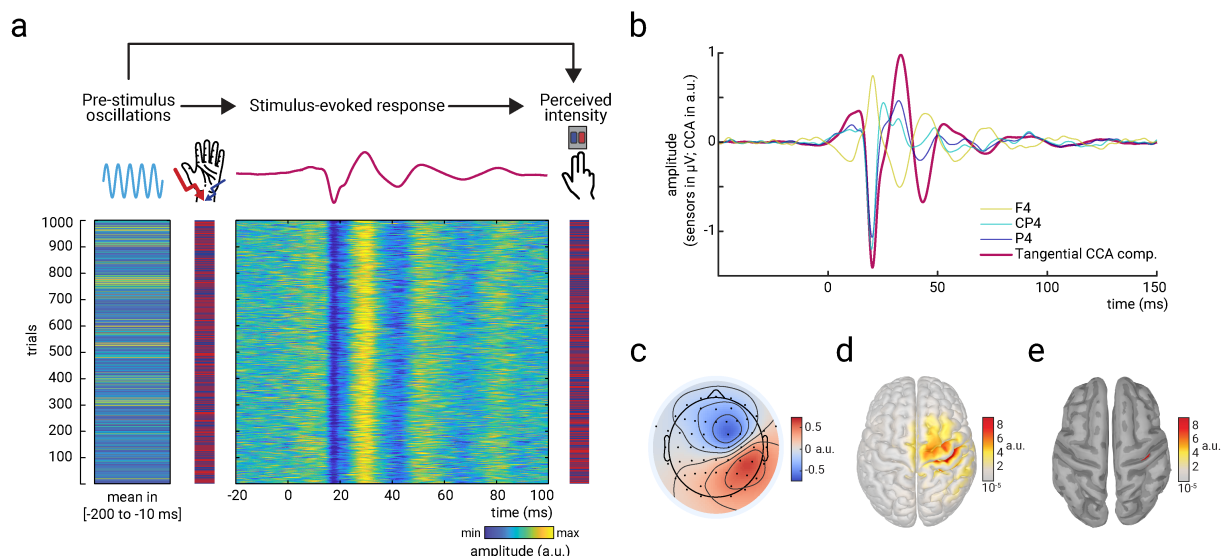68    through resting membrane potentials.



**Fig. 1.** Experimental paradigm and main electrophysiological measures. a) The relationships between pre-stimulus alpha oscillations, stimulus-evoked responses, and perceived intensity of somatosensory stimuli were examined in a continuous sequence of median nerve stimuli of two intensities with inter-stimulus intervals of ISI = 1513 ± 50 ms. After every stimulus, participants were to rate the perceived intensity as either "strong" or "weak" as fast as possible by button press. The raster plots represent the data of an exemplary subject with the rows corresponding to single trials. Displayed from left to right: Average pre-stimulus alpha amplitude, intensity of the presented stimuli (red=strong; blue=weak intensity), short-latency somatosensory evoked potentials (SEP), and the perceived intensity as reported by the participants (red=strong; blue=weak intensity). Alpha activity and the SEP were both retrieved from the *tangential CCA component* (displayed in panels b-e) and hence reflect activity of the same neuronal sources. b) Grand average of the SEP (N=32) in sensor space (electrodes F4, CP4, and P4) and for the *tangential CCA component* as derived from the single-trial extraction approach using Canonical Correlation Analysis (CCA). c) Activation pattern of the *tangential CCA component* displaying a tangential dipole contralateral to stimulation site over the central sulcus which is typical for the N20-P35 complex of the SEP. Averaged across participants (N=32). d) Neuronal sources (absolute values) underlying the activation pattern of the *tangential CCA component*, reconstructed using eLoreta inverse modeling. Averaged across participants (N=32). e) Same as d but applying an amplitude threshold of 95% in order to indicate the strongest generators of neural activity (displayed on a smoothed cortex surface).

## 2    Results

*Behavioral results*

Participants discriminated the weak and the strong stimuli with an average accuracy of $acc_{mean}$ = 69.72% ($SD$ = 7.94%; $CI_{95\%}$: [66.86%, 72.58%]), suggesting a moderate to high task difficulty. As confirmed by permutation tests, every individual participant performed better than chance level, all $p < .05$ (Bonferroni-corrected). The average discrimination sensitivity was $d'_{mean}$ = 1.14 ($SD$ = .46; $CI_{95\%}$: [0.98, 1.31]) and the average criterion $c_{mean}$ = .01 ($SD$ = .22; $CI_{95\%}$: [-.066, .094]), according to Signal Detection Theory (Green & Swets, 1966). Participants pressed the respective response button with an average reaction time of $RT_{mean}$ = 642.42 ms ($SD$ = 95.79 ms; $CI_{95\%}$: [607.89 ms, 676.96 ms]).

*Extraction of single-trial somatosensory evoked potentials*

Single-trial activity of the early SEP was extracted using a variant of Canonical Correlation Analysis (CCA; Fedele et al., 2013; Waterstraat et al., 2015), as previously reported for a similar paradigm examining the fluctuation of single-trial SEPs in response to stimuli with constant intensity (Stephani et al., 2020). This variant of CCA extracts a number of spatially distinct components based on a pattern matching between average SEP and single trials. Similar to Stephani et al. (2020), a prominent CCA component was identified in all subjects, that showed a clear peak at around 20 ms post-stimulus (Fig. 1b) and displayed the pattern of the typical N20 tangential dipole (Fig. 1c). Furthermore, neuronal sources of this CCA component were primarily located in the anterior wall of the post-central gyrus (Brodmann area 3b) in the primary somatosensory cortex (Fig. 1d & e). Single-trial SEPs from this – as is referred to in the following – *tangential CCA component* are displayed for an exemplary subject in Figure 1a.

94    *Pre-stimulus alpha amplitude is associated with a bias in perceived stimulus intensity*

95          To assess whether pre-stimulus neural states modulated the perception of upcoming

96    somatosensory stimuli, we related oscillatory activity in the alpha band (8-13 Hz) before

97    stimulus onset to the participants´ reports of perceived stimulus intensity. Alpha band activity

98    was measured from the same neural sources as the SEP, applying the spatial filters of the

99    tangential CCA component. Figure 2a shows the envelope of pre-stimulus alpha activity

100   depending on the behavioral responses of the participants. Pre-stimulus alpha amplitude was

101   higher when participants rated the stimulus to be weak rather than strong (regardless of the

102   actual stimulus intensity). This observation was further quantified with Signal Detection

103   Theory (SDT; Green & Swets, 1966) in order to differentiate the ability to discriminate

104   stimulus intensities, as measured by *sensitivity d'*, from a response bias towards either strong

105   or weak perceived intensity, as measured by *criterion c*. In correspondence with a recent

106   study in the visual domain (Iemi et al., 2017), these SDT-derived parameters were statistically

107   compared between the 20% of trials with the lowest and the 20% of trials with the highest

108   pre-stimulus alpha amplitudes (as averaged in a time window from 200 to 10 ms before the

109   stimulus onset; Fig. 2b). A paired-sample *t*-test confirmed a difference regarding *criterion c*,

110   $t(31) = -2.777, p = .009$, *Cohen´s d* $= -.491$, with average criterions of $c_{lowest20\%} = -.009$ and

111   $c_{highest20\%} = .060$ ($CI_{95\%}$ of difference: $[-.119, -.018]$). No difference was found for *sensitivity*

112   *d'*, $t(31) = -1.425, p = .164$, *Cohen´s d* $= -.252$, with average sensitivities $d'_{lowest20\%} = 1.058$

113   and $d'_{highest20\%} = 1.142$ ($CI_{95\%}$ of difference: $[-.204, .036]$). Thus, higher pre-stimulus alpha

114   amplitude was associated with a higher threshold to rate the stimulus as "strong",

115   corresponding to a bias to generally report lower stimulus intensities, whereas the

116   discriminability between the stimulus categories appeared unaffected.
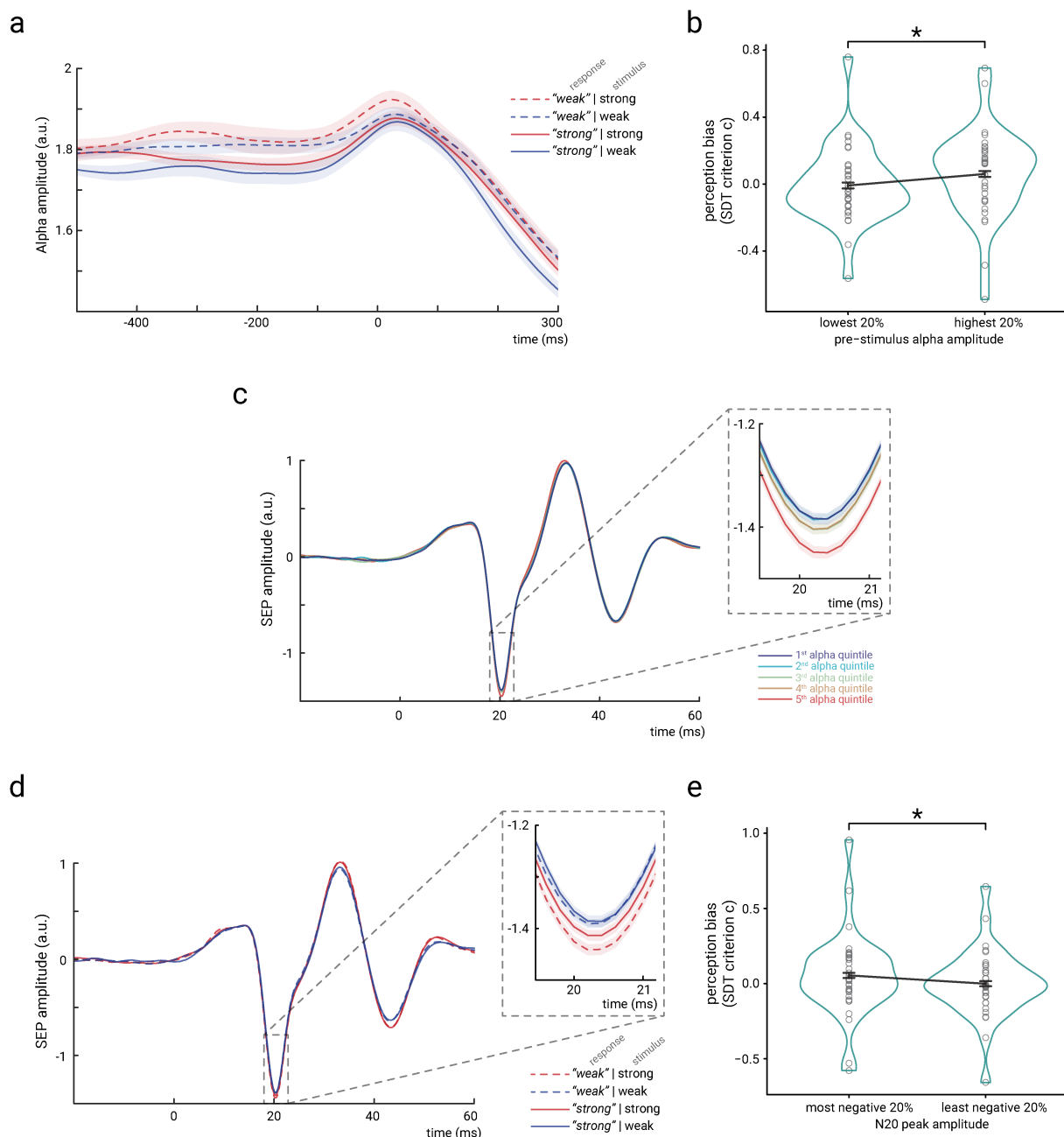
7

**Fig. 2.** Bi-variate relationships between pre-stimulus alpha amplitude, N20 peak amplitude, and perceived stimulus intensity. a) Time course of the amplitude of pre-stimulus alpha band activity (8-13 Hz) displayed by behavioral response categories. Note that for statistical analyses, pre-stimulus epochs were cut at -5 ms relative to stimulus onset *before* filtering the data in the alpha band (8-13 Hz), in order to prevent contamination of the pre-stimulus window by stimulus-related activity. b) Change in perception bias (i.e., SDT parameter *criterion c*) from the lowest to the highest alpha amplitude quintile (as measured between -200 and -10 ms). c) SEP (tangential CCA component) sorted with respect to pre-stimulus alpha amplitude quintiles. Alpha quintiles were sorted in ascending order (i.e., 1st quintile = lowest alpha amplitude). d) SEP (tangential CCA component) sorted according to behavioral response categories. e) Change in perception bias (i.e., SDT parameter *criterion c*) from the most to the least negative N20 peak amplitude quintile. All panels show the grand average across all participants (N=32). Shaded areas in panels a, c, and d, as well as error bars in panels b and e correspond to the standard errors of the mean based on the within-subject variances (Morey, 2008). Transparent circles in panels b and e reflect data of individual participants while black lines reflect the arithmetic mean on group level.

8

117   *Pre-stimulus alpha amplitude is associated with single-trial N20 amplitudes*

118   Following the hypothesis that both pre-stimulus alpha band activity and the N20

119   component of the SEP reflect changes in instantaneous cortical excitability, a covariation of

120   these two measures should be expected (Stephani et al., 2020). Indeed, higher pre-stimulus

121   alpha amplitudes were associated with larger (i.e., more negative) N20 peak amplitudes (Fig.

122   2c), as statistically tested with a random-slope linear-mixed-effects model, $\beta_{fixed}$ = -.023,

123   $t(32.17)$ = -2.969, $p$ = .006 (CI$_{95\%}$ of $\beta_{fixed}$: [-.040, -.007]). Notably, the direction of this effect

124   may appear counter-intuitive at first sight but can be explained by the physiological basis of

125   EEG generation, which offers important insights into the functional link between pre-stimulus

126   alpha activity and SEP (see Discussion section *Opposing signatures of presented stimulus*

127   *intensity and excitability in the early SEP*).

128   *Single-trial N20 amplitudes are associated with a bias in perceived stimulus intensity*

129   Given the relationships of pre-stimulus alpha activity with perceived stimulus intensity

130   and N20 peak amplitudes, we tested whether the latter also related to the SDT parameters of

131   the behavioral performance. In parallel to the analyses of the effect of pre-stimulus alpha

132   activity, *sensitivity d'* and *criterion c* were statistically compared between the 20% of trials

133   with the most negative and the 20% of trials with the least negative N20 peak amplitudes.

134   Again, a significant difference emerged for *criterion c*, $t(31)$ = 2.306, $p$ = .028, *Cohen's*

135   $d$ = .408, with average criterions of $c_{most\ neg.20\%}$ = .054 and $c_{least\ neg.20\%}$ = -.001 (CI$_{95\%}$ of

136   difference: [.006, .104]), as assessed with a paired-sample $t$-test. No effect emerged for

137   *sensitivity d'*, $t(31)$ = -1.747, $p$ = .091, *Cohen's d* = -.309, with $d'_{least\ neg.20\%}$ = 1.213 and

138   $d'_{most\ neg.20\%}$ = 1.142 (CI$_{95\%}$ of difference: [-.154, .012]). Thus, c*riterion c* was lower for less

139   negative than for more negative N20 peak amplitudes (Fig. 2e). This indicates that

140   participants were more likely to rate a stimulus as "strong" rather than "weak" when the

141   magnitude of the N20 potential was smaller (after taking into account the stimulus' actual

142    intensity), as is it also becomes evident from the SEPs sorted by the behavioral response

143    categories (Fig. 2d).

144    *Structural equation modeling of effect paths*

145         Importantly, Figure 2d also suggests that N20 amplitudes were generally larger (i.e.,

146    more negative) for higher stimulus intensities – thus showing an effect of opposite direction

147    on N20 amplitudes as compared to instantaneous cortical excitability. In order to disentangle

148    these effects of excitability and stimulus intensity, we examined their respective contributions

149    in a two-level structural equation model, with *stimulus intensity*, *pre-stimulus alpha amplitude*,

150    and *N20 peak amplitude* as predictors of *perceived stimulus intensity* on level 1 (within

151    subjects), and random intercepts as well as their variances on level 2 (between subjects),

152    including all single trials. Furthermore, we added the measures of compound nerve action

153    potentials of the median nerve (*CNAP*; Fig. 3a & 3b) and compound muscle action potentials

154    of the M. abductor pollicis brevis (*CMAP*; Fig. 3c & 3d) to the model, in order to control for
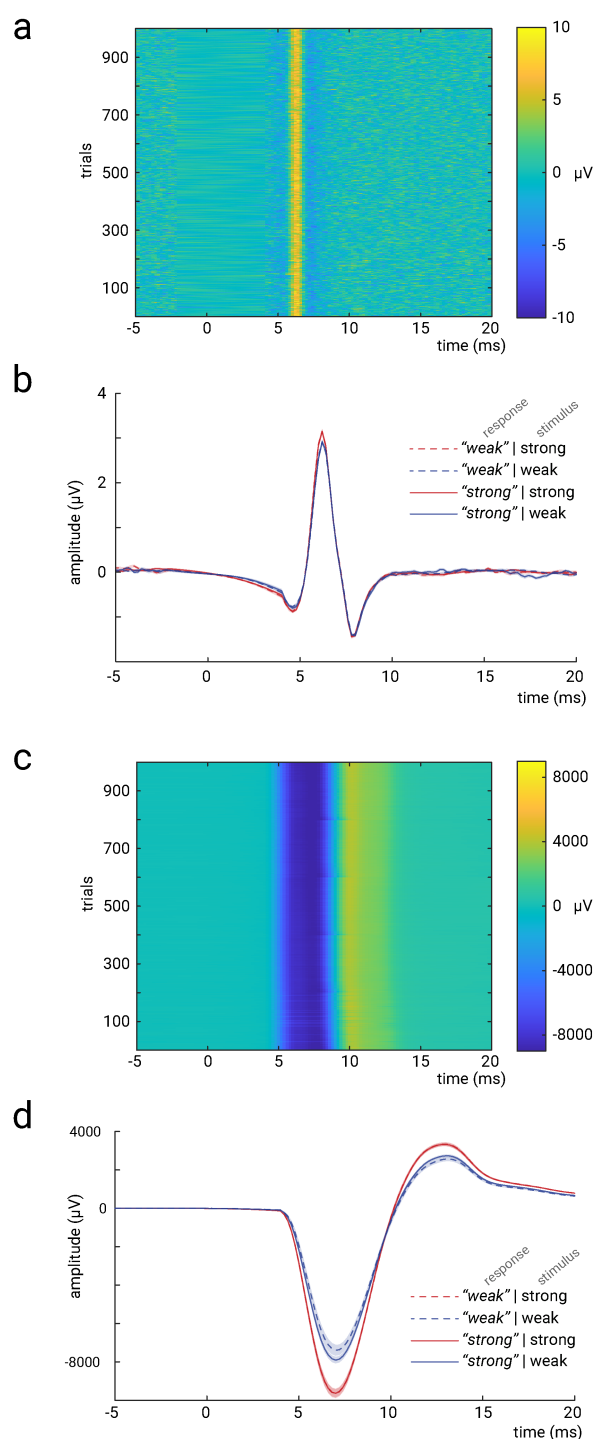
155    peripheral variability.

**Fig. 3.** Measures to control for peripheral nerve variability. a) Single trials of the *compound nerve action potential (CNAP)* in response to the median nerve stimuli, measured at the inner side of the ipsilateral upper arm (shown for an exemplary subject). b) Grand average across participants (N=32) of the CNAP, displayed by stimulus and response types. c) Single trials of the *compound muscle action potential (CMAP)*, measured at the M. abductor pollicis brevis (shown for an exemplary subject). d) Grand average across participants (N=32) of the CMAP, displayed by stimulus and response types. Shaded areas in panels b and d correspond to the standard errors of the mean based on the within-subject variances (Morey, 2008).

167        On the one hand, both these peripheral measures should relate to stimulus intensity.

168    On the other, there should be no effect of CNAP and CMAP on N20 amplitudes, when

169    statistically controlling for stimulus intensity if the hypothesized fluctuations of excitability

170    emerge on a cortical level. Yet, stimulus-induced thumb twitches may influence the

171    participants´ intensity ratings of the stimuli (even though the stimulated hand was covered

172    with a paper box). The resulting two-level structural equation model (SEM; Fig. 4) indicated

173    statistical significance of all hypothesized effect paths, all $p_\beta \leq .003$, with model fit indices of

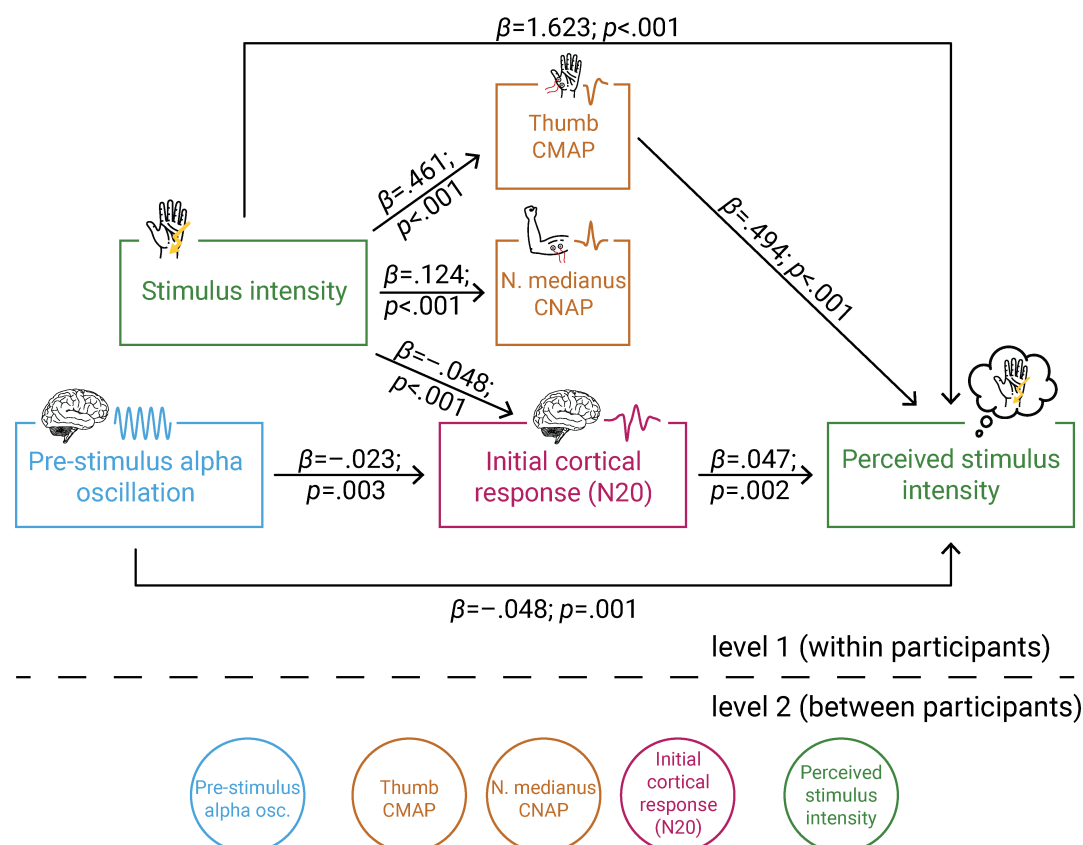174    AIC = 278788.5, BIC = 278972.2, and log-likelihood = -139372.2.



**Fig. 4.** Multi-level structural equation model of the interplay between pre-stimulus alpha activity, the initial cortical response (N20 component of the SEP), intensity of the presented stimuli, the peripheral control measures CMAP of the M. abductor pollicis brevis and CNAP of the median nerve, as well as the perceived intensity as reported by the participants. Effect paths were estimated between the manifest variables on level 1 (within participants). Latent variables on level 2 served to estimate the respective random intercepts as well as their between-subject variances according to the latent variable approach for multi-level models as implemented in *Mplus*.

175    To evaluate the model fit, we compared a list of alternative models in- or excluding

176    relevant effect paths (Table 1). As indicated by Chi-Square Difference Tests, the log-

177    likelihood of SEM 1 did not differ from those of SEMs 2-4. Seeking model parsimony, SEM

178    1 is preferred over SEMs 2-4 since the latter models included one more parameter each, while

179    fitting the data equally well. In comparison to SEMs 5-8, SEM 1 showed a significantly

180    higher log-likelihood suggesting a better model fit than these more parsimonious models. This

181     is further supported by the AIC and BIC values which were altogether lowest for SEM 1.

182     Hence, we conclude that SEM 1 fitted our empirical data best.

183     The estimated path coefficients (Fig. 4) correspond well with above reported bivariate

184     relationships: When controlling for stimulus intensity, both higher pre-stimulus alpha

185     amplitudes and more negative N20 amplitudes were associated with a lower perceived

186     intensity (equivalent to a response bias as reflected in *criterion c*), as well as higher pre-

187     stimulus alpha amplitudes co-occurred with more negative N20 amplitudes. In addition, the

188     SEM further dissociated the effects of stimulus intensity on early electrophysiological

189     measures and their respective effects on perceived stimulus intensity. Higher stimulus

190     intensity was associated with larger N20 amplitudes, which constitutes an effect of opposite

191     direction as compared to the N20-related excitability effect on perceived intensity.

192     Furthermore, higher stimulus intensity also led to larger amplitudes of CMAP and CNAP, due

193     to the physical difference in stimulation strength, as could be expected a priori. Additionally,

194     larger CMAP amplitudes resulted in a higher perceived intensity, while no such effect was

195     observed for CNAP. Importantly, neither CMAP nor CNAP related to N20 amplitudes when

196     controlling for stimulus intensity. Thus, fluctuations in cortical processing were not driven by

197     peripheral variability. Finally, a substantial effect on the perceived intensity was found for

198     stimulus intensity. This was expected as the overall accuracy in the discrimination task was

199     about 70%.

200     Taken together, the SEM confirms the hypothesized influences of instantaneous

201     fluctuations of early somatosensory evoked potentials as well as pre-stimulus oscillatory

202     activity on the consciously accessible percept of a stimulus. Moreover, this analysis

203     demonstrates that stimulus intensity and cortical excitability, which in turn determines the

204     perceived stimulus intensity, show opposing effects on the amplitude of the early SEP.

205

206

| | Model fit indices | | | | | |
|---|---|---|---|---|---|---|
| | AIC diff. | BIC diff. | LL diff. | $\chi^2$ diff. | df diff. | $p$ value |
| (1) Original SEM | | | | | | |
| (2) SEM incl. N20 ~ CNAP | 1.813 | 10.166 | 0.093 | 0.146 | -1 | .702 |
| (3) SEM incl. N20 ~ CMAP | 0.088 | 8.441 | 0.956 | 0.799 | -1 | .371 |
| (4) SEM incl. perceived_int ~ CNAP | 1.967 | 10.320 | 0.016 | 0.019 | -1 | .890 |
| (5) SEM excl. perceived_int ~ prestim | 8.002 | -0.351 | -5.001 | 11.415 | 1 | **< .001** |
| (6) SEM excl. N20 ~ prestim | 15.053 | 6.701 | -8.527 | 8.087 | 1 | **.005** |
| (7) SEM excl. N20 | 47.099 | 22.040 | -26.550 | 31.095 | 3 | **< .001** |
| (8) SEM excl. CMAP | 9586.906 | 9570.200 | -4795.453 | 87.030 | 2 | **< .001** |

**Table 1.** Model comparison of SEMs. The original SEM (1) was compared to the alternative models (2-8) using AIC, BIC, log-likelihood (LL), and the Chi-Square Difference Test based on the log-likelihood (with corresponding $p$ value). Differences in AIC, BIC, LL, and degrees of freedom (df) were derived by the subtraction *alternative SEM minus SEM 1*. A better model fit is indicated by lower AIC and/or BIC as well as higher LL. The $\chi^2$ difference tests correspond to the comparisons *model with fewer parameters minus model with more parameters*.

207    *Variability in thalamus-related activity is not related to behavioral responses*

208        To examine further whether the observed neuronal effects on the perceived stimulus

209    intensity were of a cortical origin, we analyzed the EEG responses prior to the N20 potential.

210    In a sub-sample of 13 participants, the CCA decomposition provided a component that

211    showed a clear peak at 15 ms, characterized by a spatial pattern that suggested a deep, medial

212    source (Fig. 5a & b). Most likely, this CCA component thus corresponds to the P15 potential

213    of the SEP, which is thought to reflect activity in the thalamus (Albe-Fessard et al., 1986).

214    The amplitude of this P15 component did not relate to the perceived stimulus intensity, as

215    examined with a random-intercept linear-mixed-effects model with *perceived intensity* as

216    dependent variable and *P15 amplitude* and *stimulus intensity* as predictors, $\beta_{P15} = .008$,

217    $z = 0.394$, $p = .694$ (CI$_{95\%}$ of $\beta_{P15}$: [-.031,  .047]). As expected, *stimulus intensity* however

218    showed a significant effect on *perceived intensity*, $\beta_{stim\_int} = 1.851$, $z = 46.463$, $p < .001$

219    (CI$_{95\%}$ of $\beta_{stim\_int}$: [1.773, 1.929]). Additionally, we calculated the statistical power of finding

220    an effect of P15 amplitude in the linear-mixed-effects model, using Monte Carlo simulations

221    (Green & MacLeod, 2016) and assuming an effect size comparable to the observed N20 effect

222    on perceived intensity. The post-hoc power analysis revealed a statistical power of 71.9%.

223    Therefore, we conclude that it is unlikely that the effect of N20 amplitudes on perceived

224    stimulus intensity was driven by thalamic variability and that the modulation of perceived

225    stimulus intensity emerges rather on the cortical level, reflecting instantaneous changes of
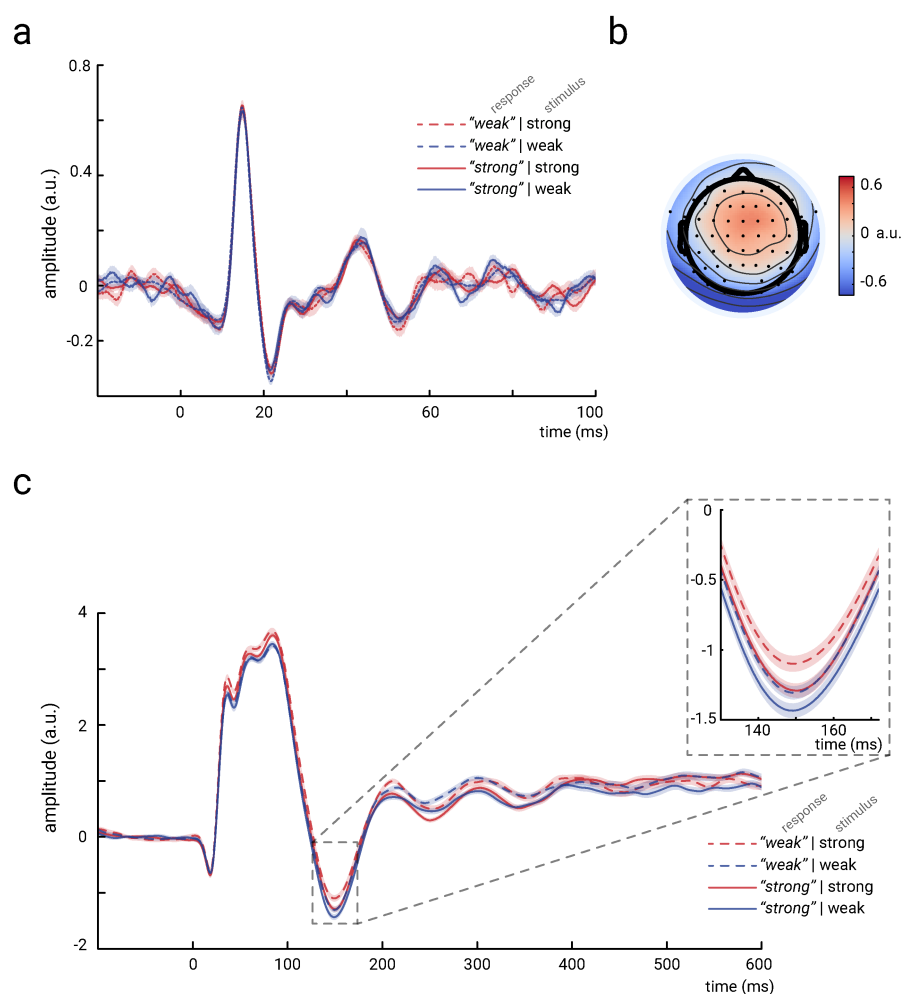
226    cortical excitability.



**Fig. 5.** Thalamic activity and later SEP components. a) Grand-average (N=13) of the thalamic CCA component, showing a clear P15 potential which did not differ across behavioral response categories. b) Activation pattern of the thalamic CCA component (average across subjects). c) Grand average (N=32) of later SEP components (extracted with the tangential-CCA filter in the frequency range from 0.5 to 45 Hz). The N140 is visible as a negative peak at around 149 ms. Larger N140 amplitudes are associated with higher perceived intensities. Shaded areas correspond to the standard errors of the mean based on the within-subject variances (Morey, 2008).

15

227    *Effects in later SEP components conform with previous studies*

228         In order to relate our novel findings in early SEPs to the existing literature on

229    somatosensory processing at later stages, we additionally examined a well-studied later

230    component of the SEP, the N140. For this SEP component, a larger amplitude has typically

231    been associated with a stronger percept of the presented stimulus (e.g., Al et al., 2020;

232    Schubert et al., 2006). Indeed, a comparable effect of N140 amplitude on perceived intensity

233    was also present in our data (Fig. 5c), as statistically tested with a random-slope linear-mixed-

234    effects model, $\beta_{\text{fixed}}$ = -.058, $z$ = -3.387, $p$ < .001 (CI$_{95\%}$ of $\beta_{\text{fixed}}$: [-.093, -.024]). Also, the

235    presented stimulus intensity was related to the perceived intensity, $\beta_{\text{fixed}}$ = 1.876, $z$ = 14.015,

236    $p$ < .001 (CI$_{95\%}$ of $\beta_{\text{fixed}}$: [1.605, 2.145]), which was expected given the participants´

237    discrimination performance being above chance level. In addition, a second random-slope

238    linear-mixed-effects model indicated that N140 amplitudes in turn modulated the presented

239    stimulus intensity, $\beta_{\text{fixed}}$ = .030, $t$(30.92) = 2.275, $p$ = .030 (CI$_{95\%}$ of $\beta_{\text{fixed}}$: [.004, .056]), as

240    well as to pre-stimulus alpha activity, $\beta_{\text{fixed}}$ = .021, $t$(31.70) = 2.73, $p$ = .030 (CI$_{95\%}$ of $\beta_{\text{fixed}}$:

241    [.002, .040]).

242         Taken together, our results are thus consistent with previous studies on the relation

243    between pre-stimulus state and somatosensory processing at later stages, while demonstrating

244    opposing effects for the very first cortical response.


245    **3     Discussion**

246         Using a somatosensory discrimination paradigm, we examined the modulation of

247    perceived stimulus intensity by instantaneous fluctuations of cortical excitability at initial

248    cortical processing. Both pre-stimulus alpha band activity and initial cortical evoked

249    responses were associated with a bias in intensity discrimination, suggesting that a lower

250    cortical excitability reduces the perceived intensity of sensory stimuli. Furthermore, we rule

251    out that variability in peripheral nerve activity accounted for these effects, in line with the

16

252    notion of instantaneous excitability changes being intrinsic to cortical brain dynamics.

253    Intriguingly, elevated excitability and higher presented stimulus intensity resulted in opposing

254    amplitude effects on the initial stimulus-related response in the cortex, the N20 component of

255    the SEP. Based on the neurophysiological principles of the EEG generation, this finding may

256    be explained by a mechanistic link between pre-stimulus alpha activity and initial cortical

257    EPSPs through modulations of resting membrane potentials.

258    *Fluctuations of cortical excitability affect the perceived stimulus intensity*

259            In line with previous studies on the modulatory role of alpha oscillations on perceptual

260    processes (Craddock et al., 2017; Iemi et al., 2017), we found higher pre-stimulus alpha

261    amplitudes to be associated with a lower perceived intensity of somatosensory stimuli. This

262    was indicated both by an increased threshold (*criterion c*) of reporting a higher stimulus

263    intensity according to Signal Detection Theory (Green & Swets, 1966), and by the negative

264    relationship between pre-stimulus alpha amplitude and reported stimulus intensity in the

265    structural equation model. Moreover, sensory processing appeared to be modulated by

266    ongoing oscillatory activity already during initial cortical responses, as suggested by the

267    relations between pre-stimulus alpha activity and N20 amplitude, as well as N20 amplitude

268    and perceived stimulus intensity. The N20 component of the SEP reflects initial stimulus-

269    related excitatory activity (i.e., excitatory post-synaptic potentials; EPSPs) resulting from the

270    first thalamo-cortical volley to the primary somatosensory cortex (Bruyns-Haylett et al., 2017;

271    Nicholson Peterson et al., 1995; Wikström et al., 1996) and thus represents a direct measure

272    of cortical excitability (when keeping the stimulus intensity constant). The modulation of

273    perceived stimulus intensity therefore relates to a sensory bias at earliest possible cortical

274    processing, reflecting fluctuations of instantaneous neural excitability.

275            Furthermore, these findings demonstrate that effects of pre-stimulus oscillatory

276    activity on the processing of sensory stimuli are not restricted to near-threshold stimuli where

17

277    a detection threshold is assumed to be shifted by ongoing brain activity (Iemi et al., 2017;

278    Samaha et al., 2020). Instead, our findings suggest that cortical excitability can affect the

279    representation of stimulus features in supra-threshold perception, too. Importantly, our

280    criterion-free discrimination paradigm of two neutral response alternatives ("strong" or

281    "weak") precluded the potential confounding effect of perceptual confidence, which has

282    recently been considered as an alternative explanation for pre-stimulus alpha effects on

283    perceptual biases (Benwell et al., 2017; Samaha et al., 2017). In our forced-choice paradigm,

284    different levels of perceptual confidence could not have influenced the intensity ratings since

285    the task was to distinguish two clearly perceptible stimuli, and not to report whether a

286    stimulus was perceived or not (as done in near-threshold paradigms). Thus, the current

287    findings unequivocally indicate – to the best of our knowledge for the first time – that pre-

288    stimulus alpha oscillations affect the behavioral outcome via a modulation of the internally

289    represented stimulus intensity.

290    *Opposing signatures of presented stimulus intensity and excitability in the early SEP*

291        Following the hypothesis of higher alpha activity being associated with lower cortical

292    excitability (Jensen & Mazaheri, 2010; Klimesch et al., 2007; Samaha et al., 2020), it may

293    seem counter-intuitive that higher alpha amplitudes were associated with larger (i.e., more

294    negative) N20 amplitudes in our data. However, as we proposed recently (Stephani et al.,

295    2020), this relationship may be explained by the neurophysiological mechanisms of EEG

296    generation. The generated voltage on the scalp, $U$, in our case relating to the N20 potential,

297    can be defined in the following way (Ilmoniemi & Sarvas, 2019; Kandel et al., 2000; Lopes

298    da Silva, 2004):

$$U \sim I * N_{neurons} * LF$$

299        where $I$ denotes the sum of local primary post-synaptic currents due to the activation

300    of a given neuron, $N_{neurons}$ the number of involved neurons, and $LF$ the lead field coefficient

18

301 projecting source activity to the electrodes on the scalp. Since the spatial arrangement of the

302 neural generators and the EEG sensors was stable across stimulation events, *LF* reflects a

303 constant in the measurement of the N20 potential. In contrast, $N_{neurons}$ should increase with

304 stimulus intensity since more nerve fibers are excited at stimulation site when applying

305 stimuli of higher currents. This should lead to an increase of SEP amplitude with stimulus

306 intensity, as reported in previous studies (Jousmäki & Forss, 1998; Klostermann et al., 1998)

307 and as was observed in the current dataset for cortical (Fig. 2d) as well as peripheral responses

308 (Fig. 3b & 3d). For constant stimulus intensity, however, $N_{neurons}$ is expected to stay

309 approximately constant and amplitudes in the EEG should primarily depend on *I*, reflecting

310 excitatory post-synaptic currents (EPSCs) in case of the N20 component. Crucially, EPSCs

311 directly depend on the electro-chemical driving forces produced by the membrane potential.

312 When moving the membrane potential towards depolarization – a state of higher excitability –

313 the electro-chemical driving force for further depolarizing inward trans-membrane currents is

314 decreased (Castro-Alamancos, 2009), which leads to smaller EPSCs (Deisz et al., 1991), and

315 should in turn result in smaller amplitudes of the scalp EEG. Assuming an inverse relationship

316 between the amplitude of alpha oscillations and neuronal excitability (as for example

317 indicated by a lower neural firing rate during higher alpha activity; Haegens et al., 2011), one

318 should hence rather expect *decreased* N20 amplitudes following *low* pre-stimulus alpha

319 activity. This is what was observed in our data when controlling for stimulus intensity (Fig. 4).

320 Moreover, the notion of smaller (i.e., less negative) N20 amplitudes reflecting a state of

321 higher excitability is corroborated by the behavioral data: When controlling for stimulus

322 intensity, we found less negative N20 amplitudes to be associated with higher perceived

323 stimulus intensity.

324 Taken together, our findings thus demonstrate that the intensity of the presented

325 stimulus and the degree of instantaneous neural excitability are jointly reflected in the early

326 SEP but with opposing signatures: While stronger stimulus intensity increases the N20

327    potential, *decreased* N20 amplitudes appear to be associated with an *increase* in excitability

328    (which in turn lead to a higher perceived stimulus intensity). This challenges the prevailing,

329    prominent assumption that the amplitude of brain potentials, especially at early processing

330    stages, reflects the coding of the perceived stimulus intensity. Rather, our findings call for a

331    more differentiated view. Although the amplitude of  early event-related potentials may

332    indeed reflect the size of the input (e.g., a stronger or weaker somatosensory stimulus), the

333    neural evaluation of this input (i.e., the perceived intensity), however, further depends on

334    internal neural states, such as neural excitability, which may even reverse the amplitude

335    effects of the input already at the earliest cortical processing stages. Crucially, our data are at

336    the same time consistent with previous studies on somatosensory processing at later stages,

337    where larger EEG potentials are typically associated with a stronger percept of a given

338    stimulus (e.g., Al et al., 2020; Schubert et al., 2006), as our analyses of the N140 component

339    showed. Thus, the present findings of opposing signatures of neural excitability and sensory

340    input appear to be a distinct characteristic of early cortical potentials, involving the first

341    bottom-up sensory processing. (We note, however, that the physiological interpretation of

342    amplitudes of later EEG potentials, such as the N140, is not as straightforward as described

343    above for the N20, since several distinct SEP components may interact (Auksztulewicz et al.,

344    2012), and excitatory and inhibitory contributions cannot be readily distinguished.)

*Origin of excitability fluctuations*

346         To further narrow down the neuronal sources that eventually led to fluctuations of the

347    perceptual outcome, we controlled for peripheral nerve variability, extracted spatially well-

348    defined EEG potentials, and examined subcortical activity.

349         Variability in afferent peripheral activity, as measured by compound nerve action

350    potentials (CNAP) at the upper arm, did not influence the perceived stimulus intensity when

351    controlling for stimulus intensity. However, a robust effect on the perceived stimulus intensity

352 was observed for efferent peripheral activity, as measured by compound muscle action

353 potentials (CMAP) of the M. abductor pollicis brevis. This may be explained by differences in

354 proprioceptive sensations associated with the thumb twitches elicited by the stimulation,

355 whose extent may depend on changes of the prevailing muscle tonus. Importantly, neither the

356 CNAP nor the CMAP measure related to cortical excitability as measured by the N20

357 component. Thus, the excitability effects in the early SEP are distinct from variability in

358 peripheral nerve activity.

359 Furthermore, pre-stimulus alpha band activity and the N20 component of the SEP

360 were retrieved from the same neuronal sources, which – as indicated by source reconstruction

361 – were localized in the primary sensory cortex, centered around the hand region of Brodmann

362 area 3b. Although one should bear in mind the limited spatial resolution of EEG, this further

363 supports the notion of excitability fluctuations in primary sensory regions of the cortex, being

364 reflected both in ongoing and evoked neural activity.

365 Another possibility is that already subcortical sources – particularly in the thalamus –

366 may play a role in modulating sensory excitability and hence shape the perceptual outcome

367 (Kosciessa et al., 2020). Yet, our analyses of the thalamus-related P15 component did not

368 support this notion. Given the acceptable statistical power of these analyses, we conclude that

369 the modulation of perceived intensity in somatosensory stimulation has its neuronal origin at

370 the cortical level.

371 However, it remains an open question whether the observed excitability changes

372 reflect local or global neural dynamics. Although there is initial evidence that cortical

373 excitability may be organized temporally in a scale-free manner (Stephani et al., 2020), which

374 may reflect an embedding into global critical-state dynamics (Avramiea et al., 2020; Beggs &

375 Plenz, 2003; Palva et al., 2013), future work has to examine the spatial organization of

376 excitability more specifically across different somatotopic projections in primary sensory

377 areas as well as across diverse brain regions.

378    *Conclusions*

379          Both ongoing oscillatory alpha activity as well as amplitude fluctuations of the first

380    cortical response shape the perceived intensity of somatosensory stimuli. These effects most

381    likely reflect instantaneous changes of cortical excitability in the primary somatosensory

382    regions of the cortex, leading to a sensory bias which manifests already during the very first

383    cortical response. Challenging the common view of how the evaluation of stimulus intensity

384    is reflected in brain potentials, cortical excitability and the presented stimulus intensity were

385    associated with opposing effects on the early SEP. We argue that this disparity may be

386    explained by a mechanistic link between ongoing oscillations and stimulus evoked activity

387    through membrane potential alterations. This sheds new light on the neural correlates of the

388    intensity encoding of somatosensory stimuli, which may well apply to other sensory domains,

389    too.

22

390 ## 4     Methods

391 *Participants*

392      A total of 32 participants (all male, mean age = 27.0 years, *SD* = 5.0) were recruited

393 from the database of the Max Planck Institute for Human Cognitive and Brain Sciences,

394 Leipzig, Germany. As assessed using the Edinburgh Handedness Inventory (Oldfield, 1971),

395 all participants were right-handed (lateralization score, *M* = +93.1, *SD* = 11.6). No participant

396 reported any neurological or psychiatric disease. All participants gave informed consent and

397 were reimbursed monetarily. The study was approved by the local ethics committee (Ethical

398 Committee at the Medical Faculty of Leipzig University, 04006 Leipzig, Germany). The

399 chosen sample size was based on previous, similar studies which yielded an appropriate

400 statistical power. (Please also note here that the estimates of the within-subject effects

401 analyzed in the current study were based on the analysis of single trials (nearly 1000 per

402 participant), ensuring a sufficiently high statistical power.)

403 *Stimuli*

404      Somatosensory stimuli were applied using electrical stimulation of the median nerve.

405 A non-invasive bipolar stimulation electrode was positioned on the left wrist (cathode

406 proximal). The electrical stimuli were designed as squared pulses of a 20- µs duration and

407 applied using a DS-7 constant-current stimulator (Digitimer, Hertfordshire, United Kingdom).

408 Stimuli of two intensities were presented, in the following referred to as *weak* and *strong*

409 stimulus. The intensity of the weak stimulus was set to 1.2 times the motor threshold, leading

410 to a clearly visible thumb twitch for every stimulus. The individual motor threshold was

411 determined as the lowest intensity for which a thumb twitch was visible to the experimenter,

412 as determined by a staircase procedure. The intensity of the strong stimulus was adjusted

413 during training blocks prior to the experiment so that it was barely above the *just-noticeable*

414 *difference*, corresponding to a discrimination sensitivity of about *d'* = 1.5 according to Signal

23

415     Detection Theory (SDT; Green & Swets, 1966). Thus, the stimulation intensities of the two

416     stimuli were only barely distinguishable (despite both being clearly perceivable), with average

417     intensities of 6.60 mA ($SD$ = 1.62) and 7.93 mA  ($SD$ = 2.06), for the weak and strong

418     stimulus, respectively.

419     *Procedure*

420         During the experiment, participants were seated comfortably in a chair their hands

421     extended in front of them in the supinate position on a pillow. The left hand and wrist, to

422     which the stimulation electrodes were attached, was covered with a paper box in order to

423     prevent the participants to judge the stimulus intensity visually by the extent of thumb

424     twitches elicited by the stimulation. Weak and strong stimuli were presented with an equal

425     probability in a continuous, pseudo-randomized sequence with inter-stimulus intervals (ISI)

426     ranging from 1463 to 1563 ms (randomly drawn from a uniform distribution;

427     $ISI_{average}$ = 1513 ms). In total, 1000 stimuli were applied, divided into five blocks of 200

428     stimuli each with short breaks in between. Participants were to indicate after each stimulus

429     whether it was the weak or strong stimulus, by button press with their right index and middle

430     fingers as fast as possible. The button assignment for weak and strong stimulus was balanced

431     across participants. Furthermore, every sequence started with a weak stimulus in order to

432     provide an anchor point for the intensity judgments (participants were informed about this).

433     While performing the discrimination task, participants were instructed to fixate their gaze on a

434     cross on a computer screen in front of them.

435         Prior to the experiment, training blocks of 15 stimuli each were run in order to

436     familiarize the participants with the task and to individually adjust the intensity of the strong

437     stimulus so that a discrimination sensitivity of about $d'$=1.5 resulted (the intensity of the weak

438     stimulus was set at 1.2 times the motor threshold for all participants). On average across

439     participants, this procedure comprised 10.5 training blocks (SD=5.8). During these training

24

440    blocks, participants were provided with visual feedback of their response accuracy. No

441    information on task performance was given during the experimental blocks.

442    *Data Acquisition*

443        EEG data were recorded from 60 Ag/AgCl electrodes at a sampling rate of 5000 Hz

444    using an 80-channel EEG system (NeurOne, Bittium, Oulu, Finland). A built-in band-pass

445    filter in the frequency range from 0.16 to 1250 Hz was used. Electrodes were mounted in an

446    elastic cap (EasyCap, Herrsching, Germany) at the international 10-10 system positions FP1,

447    FPz, FP2, AF7, AF3, AFz, AF4, AF8, F7, F5, F3, F1, Fz, F2, F4, F6, F8, FT9, FT7, FT8,

448    FT10, FC5, FC3, FC1, FC2, FC4, FC6, C5, C3, C1, Cz, C2, C4, C6, CP5, CP3, CP1, CPz,

449    CP2, CP4, CP6, T7, T8, TP7, TP8, P7, P5, P3, P1, Pz, P2, P4, P6, P8, PO7, PO3, PO4, PO8,

450    O1, and O2, with FCz as the reference and POz as the ground. For the purpose of  source

451    reconstruction, the electrode positions were measured in 3D space individually for each

452    subject using the Polhemus Patriot motion tracker (Polhemus, Colchester, Vermont). In order

453    to record the electrooculogram (EOG), four additional electrodes were positioned at the outer

454    canthus and the infraorbital ridge of each eye. The impedances of all electrodes were kept

455    below 10 kΩ. For source reconstruction, EEG electrode positions were measured in 3D space

456    individually for each subject using Polhemus Patriot (Polhemus, Colchester, Vermont).

457    Additionally, the compound nerve action potential (CNAP) of the median nerve and the

458    compound muscle action potential (CMAP) of the M. abductor pollicis brevis were measured.

459    For the CNAP, two bipolar electrodes were positioned on the inner side of the left upper arm

460    along the path of the median nerve, at a distance of about 1 cm (reference electrode distal).

461    The CMAP was measured from two bipolar electrodes placed on the stimulated hand, one on

462    the muscle belly of the M. abductor pollicis brevis and the other on the second joint of the

463    thumb (reference electrode).

464    Structural T1-weighted MRI scans (MPRAGE) of all participants but two were

465    obtained from the database of the Max Planck Institute for Human Cognitive and Brain

466    Sciences, Leipzig, Germany, acquired within the same year of the experiment or up to 3 years

467    earlier on a 3T Siemens Verio, Siemens Skyra or Siemens Prisma scanner (Siemens, Erlangen,

468    Germany).

469    *EEG pre-processing*

470    Stimulation artifacts were cut out and interpolated between -2 to 4 ms relative to

471    stimulus onset using Piecewise Cubic Hermite Interpolating Polynomials (MATLAB function

472    *pchip*). The EEG data were band-pass filtered between 30 and 200 Hz, sliding a 4$^{th}$ order

473    Butterworth filter forwards and backwards over the data to prevent phase shift (MATLAB

474    function *filtfilt*). As outlined in a previous study (Stephani et al., 2020), this filter allowed to

475    specifically focus on the N20-P35 complex of the SEP, which emerges from frequencies

476    above 35 Hz, and to omit contributions of later (slower) SEP potentials of no interest.

477    Additionally, this filter effectively served as baseline correction of the SEP since it removed

478    slow trends in the data, reaching an attenuation of 30 dB at 14 Hz, thus ensuring that

479    fluctuations in the SEP did not arise from fluctuations within slower frequencies (e.g., alpha

480    band activity). Subsequently, segments of the data that were distorted by muscle or non-

481    biological artifacts were removed by visual inspection. After re-referencing to an average

482    reference, eye artefacts were removed using independent component analysis (Infomax ICA)

483    whose weights were calculated on the data band-pass filtered between 1 and 45 Hz (4$^{th}$ order

484    Butterworth filter applied forwards and backwards). For SEP analysis, the data were

485    segmented into epochs from -100 to 600 ms relative to stimulus onset, resulting in about 995

486    trials on average per participant. EEG pre-processing was performed using EEGLAB

487    (Delorme & Makeig, 2004), and custom written scripts in MATLAB (The MathWorks Inc.,

488    Natick, Massachusetts).

489    *Single-trial extraction using CCA*

490         Single-trial SEPs were extracted using Canonical Correlation Analysis (CCA), as

491    proposed by Waterstraat et al. (2015), and in the same way applied as described in Stephani et

492    al. (2020) for a similar dataset.

493         CCA finds the spatial filters $\boldsymbol{w}_x$ and $\boldsymbol{w}_y$ for multi-channel signals $\boldsymbol{X}$ and $\boldsymbol{Y}$ by solving

494    the following optimization problem for maximizing the correlation:

$$\max_{w_x, w_y} corr(\boldsymbol{w}_x^T \boldsymbol{X}, \boldsymbol{w}_y^T \boldsymbol{Y})$$

495    where $\boldsymbol{X}$ is a multi-channel signal constructed from concatenating all the epochs of a subject's

496    recording, i.e. $\boldsymbol{X} = [\boldsymbol{x}_1, \boldsymbol{x}_2, \dots, \boldsymbol{x}_N]$ with $\boldsymbol{x}_i \in \mathbb{R}^{channel \times time}$ being the multi-channel signal of

497    a single trial and $N$ the total number of trials. Additionally, $\boldsymbol{Y} = \underbrace{[\overline{\boldsymbol{x}}, \dots, \overline{\boldsymbol{x}}]}_{N \ times}$ with $\overline{\boldsymbol{x}} = \frac{1}{N} \sum_{i=1}^{N} \boldsymbol{x}_i$

498    denoting the grand average of all trials. Since averaging cancels the background noise and

499    recovers the shared morphology of the SEP of interest among all the trials, the CCA

500    procedure resembles a template matching between the single trial signals and the template

501    time signature of the SEP of interest. The spatial filter $\boldsymbol{w}_x$ provides us with a vector of

502    weights for mixing the channels of each single trial (i.e. $\boldsymbol{x}_{i,CCA} = \boldsymbol{w}_x^T \boldsymbol{x}_i$) and recovering their

503    underlying SEP. Therefore, $\boldsymbol{w}_x$ can be interpreted as the spatial signature of the SEP of

504    interest across all single trials. The optimization problem of CCA can be solved using

505    eigenvalue decomposition. Therefore, multiple CCA spatial components can be extracted for

506    each subject, being the eigenvectors of the corresponding eigenvalue decomposition. Since we

507    are mainly interested in the early portion of the SEP, the two signal matrices $\boldsymbol{X}$ and $\boldsymbol{Y}$ were

508    constructed using shorter segments from 5 to 80 ms post-stimulus. The extracted CCA spatial

509    filter was, however, applied to the whole-length epochs from -100 to 600 ms. The signal

510    resulting from mixing the single trial's channels using the CCA spatial filter $\boldsymbol{w}_x$,

511    i.e. $\boldsymbol{x}_{i,CCA} = \boldsymbol{w}_x^T \boldsymbol{x}_i$, is called a CCA component of that trial.

512    The spatial activity pattern of each CCA component was computed by multiplying the

513    spatial filters $\boldsymbol{w}_x$ by the covariance matrix of $\boldsymbol{X}$, as $cov(\boldsymbol{X})\boldsymbol{w}_x$, in order to take the noise

514    structure of the data into account (Haufe et al., 2014). The CCA components whose spatial

515    patterns showed a pattern of a tangential dipole over the central sulcus (typical for the N20-

516    P35 complex) were selected for further analyses and referred to as *tangential CCA*

517    *components*. Such a tangential CCA component was present in all subjects among the first

518    two CCA components with the maximum canonical correlation coefficients. Since CCA

519    solutions are insensitive to the polarity of the signal, we standardized the resulting tangential

520    CCA components by multiplying the spatial filter by a sign factor, in the way that the N20

521    potential always appeared as a negative peak in the SEP.

522    Furthermore, in a sub-sample of 13 subjects, a CCA component could be identified

523    among the first four CCA components, that showed a peak at around 15 ms post-stimulus

524    (presumably the P15 component of the SEP) and a spatial pattern that was characterized by a

525    central, outspread activation (in the following referred to as *thalamic CCA component*). Also

526    here, the CCA components were standardized so that the P15 always appeared as a positive

527    peak.

528    In order to additionally evaluate the later time course of the SEP (i.e., the lower and

529    later frequency content), the spatial filter of the tangential CCA component was applied to

530    EEG data temporally filtered between 0.5 and 45 Hz (apart from this, preprocessed in the

531    same way as described above).

532    *SEP peak amplitudes and pre-stimulus oscillatory activity*

533    N20 peak amplitudes were defined as the minimum value in single-trial SEPs of the

534    tangential CCA components ±2 ms around the latency of the N20 in the within-subject

535    average SEP. P15 amplitudes were measured from the thalamic CCA components as the

536    average amplitude in a time window ±1 ms around the latency of the P15 in the within-subject

537    average SEP. N140 amplitudes were measured from the low-frequency-filtered EEG (0.5 to

538    45 Hz), after application of the tangential CCA filter, as the average voltage in a time window

539    between 140 and 160 ms after stimulus onset.

540         To estimate the average amplitude of pre-stimulus alpha band activity, the data were

541    segmented from -500 to -5 ms relative to stimulus onset and band-pass filtered between 8 and

542    13 Hz, using a 4$^{th}$ order Butterworth filter (applied forwards and backwards). In order to avoid

543    filter-related edge artifacts, the data segments were mirrored before filtering to both sides

544    (symmetric padding). Segmenting the data before filtering prevented any leakage from post-

545    stimulus signals to the pre-stimulus time window. In order to examine pre-stimulus alpha

546    band activity of the same sources as of the SEP, the spatial filter of the tangential CCA

547    component was also applied to the pre-stimulus alpha data. Subsequently, the amplitude

548    envelope of the extracted alpha oscillations was computed by taking the absolute value of the

549    analytic signal, using Hilbert transform of the real-valued signal. To derive one pre-stimulus

550    alpha metric for every trial, amplitudes of the alpha envelope were averaged in the pre-

551    stimulus time window of interest between -200 and -10 ms and log-transformed for

552    subsequent statistical analyses in order to approximate a normal distribution.

553    *EEG source reconstruction*

554         Sources of the EEG signal were reconstructed using lead field matrices based on

555    individual brain anatomies and individually measured electrode positions. Structural T1-

556    weighted MRI images (MPRAGE) were segmented using the Freesurfer software

557    (http://surfer.nmr.mgh.harvard.edu/), and a three-shell boundary element model (BEM) based

558    on the segmented MRI was used to compute the lead field matrix with OpenMEEG (Gramfort

559    et al., 2010; Kybic et al., 2005). A template brain anatomy (ICBM152; Fonov et al., 2009)

560    was used for two subjects for whom no individual MRI scans were available. Additionally,

561    standard electrode positions were used for one subject for whom the 3D digitization of the

562    electrode positions was corrupted. The lead field matrices were inverted using the eLORETA

563    method (Pascual-Marqui, 2007), and sources were reconstructed for the spatial patterns of the

564    tangential CCA component of every subject. For group-level analysis, we projected the

565    individual source estimates onto the ICBM152 template anatomy using the spherical co-

566    registration with the FSAverage template (Fischl et al., 1999) derived from Freesurfer.

567    Subsequently, the source estimates were averaged across subjects. Brainstorm (Tadel et al.,

568    2011) was used for building individual head models and visualizing the source space data.

569    The MATLAB implementation of the eLORETA algorithm was derived from the MEG/EEG

570    Toolbox of Hamburg (METH; https://www.uke.de/english/departments-

571    institutes/institutes/neurophysiology-and-pathophysiology/research/research-

572    groups/index.html).

573    *Processing of peripheral electrophysiological data (median nerve CNAP and thumb CMAP)*

574        Analogously to the EEG data, stimulation artifacts were cut out and interpolated

575    between -2 to 4 ms relative to stimulus-onset using Piecewise Cubic Hermite Interpolating

576    Polynomials. To achieve a sufficient signal-to-noise ratio (SNR) of the short-latency CNAP

577    peak of only a few milliseconds duration on single-trial level, the data were high-pass filtered

578    at 70 Hz (4th order Butterworth filter applied forwards and backwards). For the CMAP, no

579    further filtering was necessary given the naturally high SNR of muscle potentials (mV range).

580    Here, only a baseline correction was performed from -20 to -5 ms to account for slow

581    potential shifts. For the CNAP, single-trial peak amplitudes were extracted as the maximum

582    amplitude ±1 ms around the participant-specific latency of the CNAP peak that was found

583    between 5 and 9 ms in the within-participant averages. The CMAP was evaluated regarding

584    its peak-to-peak amplitude, which was defined as the difference between the minimum and

585    maximum amplitude measured ±1 ms around the participant-specific latencies of the negative

586     and positive peaks of the biphasic CMAP response (which were found between 5 and 11 ms

587     as well as 10 to 20 ms in the within-participant averages, respectively).

588     *Signal Detection Theory (SDT)*

589         In order to separate the discrimination ability of the two stimulus intensities from a

590     general response bias, we applied Signal Detection Theory (SDT; Green & Swets, 1966;

591     Kingdom & Prins, 2016). The ability to discriminate the two stimulus intensities was

592     quantified using *sensitivity d'*, as calculated in the following way:

$$d' = \phi^{-1}(p(\text{"strong"} \mid strong)) - \phi^{-1}(p(\text{"strong"} \mid weak))$$

593     where $\phi^{-1}$ corresponds to the inverse of the cumulative normal distribution,

594     $p(\text{"strong"} \mid strong)$ to the probability of strong stimuli being rated as strong stimuli, and

595     $p(\text{"strong"} \mid weak)$ to the probability of weak stimuli being rated as strong stimuli.

596     Response probabilities were calculated as the number of responses divided by the number of

597     stimuli of the respective categories. The response bias, *criterion c*, was calculated as follows:

$$c = -0.5 * (\phi^{-1}(p(\text{"strong"} \mid strong)) + \phi^{-1}(p(\text{"strong"} \mid weak))) \,.$$

599         According to Signal Detection Theory, *sensitivity d'* here represents the distance

600     between the distributions of the internal responses of the two stimuli, and thus reflects the

601     discriminability between strong and weak stimulus intensity. *Criterion c* reflects the internal

602     threshold above which a stimulus is rated as strong stimulus and below which a stimulus is

603     rated as weak stimulus, thus representing a general response bias. With respect to our data, a

604     higher *criterion c* therefore indicates a general tendency to report lower stimulus intensities.

605     *Statistical analyses*

606         To confirm that task accuracy was above chance level, we ran non-parametric

607     permutation tests (Crowley, 1992). Within each participant, we derived a null distribution of

608     chance-level performance by randomly remapping the behavioral responses with the

609     presented stimuli 100,000 times (Combrisson & Jerbi, 2015). The *p* value of the empirical

31

610　task accuracy was calculated as the proportion of higher accuracy values in the surrogate data.

611　Bonferroni correction was applied to account for the multiple tests across participants.

612　　　The effects of the SEP measures *pre-stimulus alpha amplitude* and *N20 peak*

613　*amplitude* on the SDT measures *sensitivity d'* and *criterion c* were examined using a binning

614　approach: First, trials were sorted according to the amplitudes of the EEG measures. Next, the

615　SDT measures corresponding to the first and fifth quintile of the sorted trials were compared

616　using paired-sample *t*-tests. To quantify effect sizes, *Cohen´s d* was calculated as the mean

617　difference between the dependent samples divided by the standard deviation of differences

618　between the dependent samples.

619　　　The relationship between pre-stimulus alpha activity and the N20 component was

620　tested using a random-slope linear mixed effects model with *pre-stimulus alpha amplitude* as

621　predictor of *N20 peak amplitude*, and *subject* as random factor:

622　　　*N20 peak amplitude ~ 1 + pre-stimulus alpha + (1 + pre-stimulus alpha | subject)* .

623　　　The relationship between thalamus-related activity and intensity perception was tested

624　using a random-intercept linear-mixed-effects model with *P15 amplitude* and *presented*

625　*stimulus intensity* as predictors of *perceived stimulus intensity*, as well as *subject* as random

626　factor:

627　　　*Perceived stimulus intensity ~ 1 + P15 amplitude + presented stimulus intensity + (1 | subject)* .

628　　　Here, a logit link function was used to account for the dichotomous scale of *perceived*

629　*stimulus intensity* (note that we refrained from estimating a random slope for P15 amplitude

630　here given the small sample size of available data for thalamic activity). Analogously, we

631　analyzed the effect of N140 amplitude on perceived stimulus intensity, however now

632　including a random slope for N140 amplitude:

633      *Perceived stimulus intensity ~ 1 + N140 amplitude + presented stimulus intensity*

634           *+ (1 + N140 amplitude + presented stimulus intensity | subject) .*

635      The dependence of the N140 on presented stimulus intensity and pre-stimulus alpha

636 activity was examined using the following model:

637      *N140 amplitude ~ 1 + pre-stimulus alpha + presented stimulus intensity*

638           *+ (1 + pre-stimulus alpha + presented stimulus intensity | subject) .*

639      Furthermore, we conducted a post-hoc power analysis to evaluate the probability of

640 finding an effect of P15 amplitude on perceived stimulus intensity if it was existent. For this,

641 we used Monte Carlo simulations with 1000 permutations based on the empirical dataset

642 (Green & MacLeod, 2016), assuming an effect size of $\beta = .05$, which is in the range of the

643 observed effect of N20 amplitude on perceived stimulus intensity.

644      In addition, the interrelation of pre-stimulus alpha activity, the N20 component of the

645 SEP, peripheral nerve activity as measured by CNAP and CMAP, the presented stimulus

646 intensity, as well as the perceived stimulus intensity were examined using confirmatory path

647 analysis based on multi-level structural equation modeling as implemented in the general

648 latent variable framework of *Mplus* (Muthén & Muthén, 1998-2017). *Pre-stimulus alpha*

649 *amplitude* and *presented stimulus intensity* were included as exogenous variables, *N20 peak*

650 *amplitude*, *CNAP amplitude*, *CMAP amplitude*, and *perceived stimulus intensity* as

651 endogenous variables. The relationships contained in the hypothesized model are summarized

652 in Table 2. Trials with no behavioral response were excluded from the analysis. In total,

653 31,347 single trials were included in the SEM, with 979.6 trials on average per participant.

654 Model parameters were estimated using the MLR estimator provided by *Mplus*, a maximum-

655 likelihood estimator robust to violations of the assumption of normally distributed data. A

656 logit link function was used to account for the dichotomous scale of *perceived stimulus*

657 *intensity*. The fit of the hypothesized model was examined comparing it to alternative models

658 constructed by stepwise in- or excluding relevant effect paths (Table 1). Model comparisons

33

659    were evaluated using $\chi^2$ difference tests based on the log-likelihood (Muthén, 1998-2004), the

660    Akaike Information Criterion (AIC), and the Bayesian Information Criterion (BIC). (Note that

661    no other fit indices, such as CFI, RMSEA or SRMR are available for our type of model with a

662    multi-level structure and a dichotomous outcome variable.)

---

Level 1 (within participants):

    N20 amplitude ~ 1 + stimulus intensity + pre-stimulus alpha

    CNAP ~ 1 + stimulus intensity

    CMAP ~ 1 + stimulus intensity

    Perceived intensity ~ 1 + stimulus intensity + N20 amplitude + pre-stimulus alpha + CMAP

Level 2 (between participants):

    N20 amplitude ~~ N20 amplitude

    CNAP ~~ CNAP

    CMAP ~~ CMAP

    Perceived intensity ~~ perceived intensity

    Pre-stimulus alpha ~~ pre-stimulus alpha

---

**Table 2.** Relationships included in the hypothesized SEM. Level 1 equations reflect the within-participant effects between variables of interest. On level 2, only intercepts and variances of each variable were modelled; apart from *stimulus intensity* which only varied within participants by experimental design.

663    For all analyses, the statistical significance level was set to *p* = .05 (two-sided).

664    Correspondingly, two-sided confidence intervals were calculated with a confidence level

665    of .95 (CI$_{95\%}$). The permutation-based analyses and *t*-tests were performed in MATLAB

666    (version 2019b, The MathWorks Inc., Natick, Massachusetts). For both the linear-mixed-

667    effects model and the structural equation models, all continuous variables (i.e., pre-stimulus

668    alpha, N20 amplitude, CNAP, and CMAP) were z-transformed prior to statistics. The linear-

669    mixed-effects model was calculated in R (version 3.5.3, R Core Team, 2018) with the *lmer*

670    function of the *lme4* package (version 1.1-23, Bates et al., 2015), estimating the fixed-effect

671     coefficients based on Maximum Likelihood (ML). To derive a *p* value for the fixed-effect

672     coefficients, the denominator degrees of freedom were adjusted using Satterthwaite´s method

673     (Satterthwaite, 1946) as implemented in the R package *lmerTest* (version 3.1-2, Kuznetsova et

674     al., 2017). Structural equation modelling was performed in *Mplus* (version 8.4 Demo, Base

675     Program and Combination Add-On; Muthén & Muthén, 1998-2017) using the

676     *MplusAutomation* package in R for scripting (Hallquist & Wiley, 2018). Post-hoc statistical

677     power analyses were performed using the R package *simr* (Green & MacLeod, 2016).

678     *Data availability*

679          The data that supports the findings of this study are available upon request from the

680     corresponding author (T.S.; stephani@cbs.mpg.de). The data cannot be made available in a

681     public repository due to the privacy policies for human biometric data according to the

682     European General Data Protection Regulation (GDPR).

683     *Code availability*

684          The custom-written code that was used for data processing and statistical analyses is

685     publicly available at https://osf.io/v9xa6/?view_only=3428139b7ab94824bac0eff0b4b92cc5.

## Acknowledgements

## Author contributions

T.S., V.V.N., and A.V. designed research; T.S. performed research; T.S. and A.H. analyzed data; T.S. wrote the first draft of the paper; T.S. and V.V.N. wrote the paper; T.S., A.H., M.J.I., A.V., and V.V.N. edited the paper; M.J.I. contributed unpublished reagents/analytic tools.

## Competing Interests statement

The authors declare no competing financial interests.

# References

Al, E., Iliopoulos, F., Forschack, N., Nierhaus, T., Grund, M., Motyka, P., Gaebler, M., Nikulin, V. V., & Villringer, A. (2020). Heart–brain interactions shape somatosensory perception and evoked potentials. *Proceedings of the National Academy of Sciences of the United States of America*, *7*, 201915629.

Albe-Fessard, D., Tasker, R., Yamashiro, K., Chodakiewitz, J., & Dostrovsky, J. (1986). Comparison in man of short latency averaged evoked potentials recorded in thalamic and scalp hand zones of representation. *Electroencephalography and Clinical Neurophysiology/Evoked Potentials Section*, *65*, 405–415.

Allison, T., McCarthy, G., Wood, C. C., & Jones, S. J. (1991). Potentials Evoked in Human and Monkey Cerebral Cortex by Stimulation of the Median Nerve. *Brain*, *114*, 2465–2503.

Arieli, A., Sterkin, A., Grinvald, A., & Aertsen, A. (1996). Dynamics of ongoing activity: Explanation of the large variability in evoked cortical responses. *Science*, *273*, 1868–1871.

Auksztulewicz, R., Spitzer, B., & Blankenburg, F. (2012). Recurrent neural processing and somatosensory awareness. *The Journal of Neuroscience*, *32*, 799–805.

Avramiea, A.-E., Hardstone, R., Lueckmann, J.-M., Bím, J., Mansvelder, H. D., & Linkenkaer-Hansen, K. (2020). Pre-stimulus phase and amplitude regulation of phase-locked responses are maximized in the critical state. *eLife*, *9*, e53016.

Bates, D., Mächler, M., Bolker, B., & Walker, S. (2015). Fitting Linear Mixed-Effects Models Using lme4. *Journal of Statistical Software*, *67*, 1–48.

Baumgarten, T. J., Schnitzler, A., & Lange, J. (2016). Prestimulus Alpha Power Influences Tactile Temporal Perceptual Discrimination and Confidence in Decisions. *Cerebral Cortex*, *26*, 891–903.

Beggs, J. M., & Plenz, D. (2003). Neuronal Avalanches in Neocortical Circuits. *The Journal of Neuroscience, 23*, 11167–11177.

Benwell, C. S. Y., Tagliabue, C. F., Veniero, D., Cecere, R., Savazzi, S., & Thut, G. (2017). Prestimulus EEG power predicts conscious awareness but not objective visual performance. *eNeuro*, *4*, ENEURO.0182-17.2017.

Bollimunta, A., Mo, J., Schroeder, C. E., & Ding, M. (2011). Neuronal mechanisms and attentional modulation of corticothalamic α oscillations. *The Journal of Neuroscience*, *31*, 4935–4943.

Bruyns-Haylett, M., Luo, J., Kennerley, A. J., Harris, S., Boorman, L., Milne, E., Vautrelle, N., Hayashi, Y., Whalley, B. J., Jones, M., Berwick, J., Riera, J., & Zheng, Y. (2017). The neurogenesis of P1 and N1: A concurrent EEG/LFP study. *NeuroImage*, *146*, 575–588.

Busch, N. A., Dubois, J., & VanRullen, R. (2009). The phase of ongoing EEG oscillations predicts visual perception. *The Journal of Neuroscience*, *29*, 7869–7876.

Castro-Alamancos, M. A. (2009). Cortical up and activated states: implications for sensory information processing. *The Neuroscientist*, *15*, 625–634.

Combrisson, E., & Jerbi, K. (2015). Exceeding chance level by chance: The caveat of theoretical chance levels in brain signal classification and statistical assessment of decoding accuracy. *Journal of neuroscience methods*, *250*, 126–136.

Craddock, M., Poliakoff, E., El-Deredy, W., Klepousniotou, E., & Lloyd, D. M. (2017). Pre-stimulus alpha oscillations over somatosensory cortex predict tactile misperceptions. *Neuropsychologia*, *96*, 9–18.

Crowley, P. (1992). Resampling Methods for Computation-Intensive Data Analysis in Ecology and Evolution. *Annual Review of Ecology and Systematics*, *23*, 405–447.

Deisz, R. A., Fortin, G., & Zieglgansberger, W. (1991). Voltage dependence of excitatory postsynaptic potentials of rat neocortical neurons. *Journal of neurophysiology*, *65*, 371–382.

Delorme, A., & Makeig, S. (2004). EEGLAB: An open source toolbox for analysis of single-trial EEG dynamics including independent component analysis. *Journal of neuroscience methods*, *134*, 9–21.

Fedele, T., Scheer, H.-J., Burghoff, M., Waterstraat, G., Nikulin, V. V., & Curio, G. (2013). Distinction between added-energy and phase-resetting mechanisms in non-invasively detected somatosensory evoked responses. *Conference proceedings: IEEE Engineering in Medicine and Biology Society. Annual Conference*, *2013*, 1688–1691.

Fischl, B., Sereno, M. I., Tootell, R. B.H., & Dale, A. M. (1999). High-resolution intersubject averaging and a coordinate system for the cortical surface. *Human Brain Mapping*, *8*, 272–284.

Fonov, V. S., Evans, A. C., McKinstry, R. C., Almli, C. R., & Collins, D. L. (2009). Unbiased nonlinear average age-appropriate brain templates from birth to adulthood. *NeuroImage*, *47*, S102.

Forschack, N., Nierhaus, T., Müller, M. M., & Villringer, A. (2020). Dissociable neural correlates of stimulation intensity and detection in somatosensation. *NeuroImage*, 116908.

Gramfort, A., Papadopoulo, T., Olivi, E., & Clerc, M. (2010). OpenMEEG: opensource software for quasistatic bioelectromagnetics. *Biomedical engineering online*, *9*, 45.

Green, D. M., & Swets, J. A. (1966). *Signal detection theory and psychophysics*. New York, NY: Wiley.

Green, P., & MacLeod, C. J. (2016). SIMR an R package for power analysis of generalized linear mixed models by simulation. *Methods in Ecology and Evolution*, *7*, 493–498.

Haegens, S., Nácher, V., Luna, R., Romo, R., & Jensen, O. (2011). α-Oscillations in the monkey sensorimotor network influence discrimination performance by rhythmical inhibition of neuronal spiking. *Proceedings of the National Academy of Sciences of the United States of America*, *108*, 19377–19382.

Hallquist, M. N., & Wiley, J. F. (2018). MplusAutomation: An R Package for Facilitating Large-Scale Latent Variable Analyses in Mplus. *Structural Equation Modeling: A Multidisciplinary Journal*, *25*, 621–638.

Haufe, S., Meinecke, F., Görgen, K., Dähne, S., Haynes, J.-D., Blankertz, B., & Bießmann, F. (2014). On the interpretation of weight vectors of linear models in multivariate neuroimaging. *NeuroImage*, *87*, 96–110.

Iemi, L., Chaumon, M., Crouzet, S. M., & Busch, N. A. (2017). Spontaneous Neural Oscillations Bias Perception by Modulating Baseline Excitability. *The Journal of Neuroscience*, *37*, 807–819.

Ilmoniemi, R., & Sarvas, J. (2019). *Brain signals: Physics and mathematics of MEG and EEG*. Cambridge: The MIT Press.

Jensen, O., & Mazaheri, A. (2010). Shaping functional architecture by oscillatory alpha activity: Gating by inhibition. *Frontiers in human neuroscience*, *4*, 186.

Jousmäki, V., & Forss, N. (1998). Effects of stimulus intensity on signals from human somatosensory cortices. *Neuroreport*, *9*, 3427–3431.

Kandel, E. R., Schwartz, J. H., & Jessell, T. M. (Eds.) (2000). *Principles of neural science.* (4. ed.). New York, NY: McGraw-Hill Health Professions Division.

Kingdom, F. A. A., & Prins, N. (2016). *Psychophysics: A practical introduction.* (Second edition). Elsevier science & technology books. London: Elsevier Academic Press.

Klimesch, W., Sauseng, P., & Hanslmayr, S. (2007). EEG alpha oscillations: The inhibition-timing hypothesis. *Brain research reviews*, *53*, 63–88.

Klostermann, F., Nolte, G., Losch, F., & Curio, G. (1998). Differential recruitment of high frequency wavelets (600 Hz) and primary cortical response (N20) in human median nerve somatosensory evoked potentials. *Neuroscience letters*, *256*, 101–104.

Kosciessa, J. Q., Lindenberger, U., & Garrett, D. D. (2020). Thalamocortical excitability adjustments guide human perception under uncertainty. *bioRxiv*.

Kuznetsova, A., Brockhoff, P. B., & Christensen, R. H. B. (2017). lmerTest Package: Tests in Linear Mixed Effects Models. *Journal of Statistical Software*, *82*, 1–26.

Kybic, J., Clerc, M., Abboud, T., Faugeras, O., Keriven, R., & Papadopoulo, T. (2005). A common formalism for the Integral formulations of the forward EEG problem. *IEEE Transactions on Medical Imaging*, *24*, 12–28.

Lakatos, P., Shah, A. S., Knuth, K. H., Ulbert, I., Karmos, G., & Schroeder, C. E. (2005). An oscillatory hierarchy controlling neuronal excitability and stimulus processing in the auditory cortex. *Journal of neurophysiology*, *94*, 1904–1911.

Lopes da Silva, F. (2004). Functional localization of brain sources using EEG and/or MEG data: volume conductor and source models. *Magnetic resonance imaging*, *22*, 1533–1538.

Morey, R. D. (2008). Confidence Intervals from Normalized Data: A correction to Cousineau (2005). *Tutorial in Quantitative Methods for Psychology*, *4*, 61–64.

Müller, N., Keil, J., Obleser, J., Schulz, H., Grunwald, T., Bernays, R.-L., Huppertz, H.-J., & Weisz, N. (2013). You can't stop the music: reduced auditory alpha power and coupling between auditory and memory regions facilitate the illusory perception of music during noise. *NeuroImage*, *79*, 383–393.

Muthén, B. O. (1998-2004). *Mplus Technical Appendices*. Los Angeles, CA: Muthén & Muthén.

Muthén, L. K., & Muthén, B. O. (1998-2017). *Mplus User´s Guide. Eighth Edition*. Los Angeles, CA: Muthén & Muthén.

Nicholson Peterson, N., Schroeder, C. E., & Arezzo, J. C. (1995). Neural generators of early cortical somatosensory evoked potentials in the awake monkey. *Electroencephalography and Clinical Neurophysiology/Evoked Potentials Section*, *96*, 248–260.

Oldfield, R. C. (1971). The assessment and analysis of handedness: The Edinburgh inventory. *Neuropsychologia*, *9*, 97–113.

Palva, J. M., Zhigalov, A., Hirvonen, J., Korhonen, O., Linkenkaer-Hansen, K., & Palva, S. (2013). Neuronal long-range temporal correlations and avalanche dynamics are correlated with behavioral scaling laws. *Proceedings of the National Academy of Sciences of the United States of America*, *110*, 3585–3590.

Pascual-Marqui, R. D. (2007). Discrete, 3D distributed linear imaging methods of electric neuronal activity. Part 1: exact, zero error localization. *arXiv*.

R Core Team (2018). *R: A language and environment for statistical computing*: R Foundation for Statistical Computing, Vienna, Austria.

Romei, V., Brodbeck, V., Michel, C., Amedi, A., Pascual-Leone, A., & Thut, G. (2008). Spontaneous fluctuations in posterior alpha-band EEG activity reflect variability in excitability of human visual areas. *Cerebral Cortex*, *18*, 2010–2018.

Samaha, J., Iemi, L., Haegens, S., & Busch, N. A. (2020). Spontaneous Brain Oscillations and Perceptual Decision-Making. *Trends in cognitive sciences*, *24*, 639–653.

Samaha, J., Iemi, L., & Postle, B. R. (2017). Prestimulus alpha-band power biases visual discrimination confidence, but not accuracy. *Consciousness and cognition*, *54*, 47–55.

Satterthwaite, F. E. (1946). An Approximate Distribution of Estimates of Variance Components. *Biometrics Bulletin*, *2*, 110.

Schubert, R., Blankenburg, F., Lemm, S., Villringer, A., & Curio, G. (2006). Now you feel it--now you don't: ERP correlates of somatosensory awareness. *Psychophysiology*, *43*, 31–40.

Stephani, T., Waterstraat, G., Haufe, S., Curio, G., Villringer, A., & Nikulin, V. V. (2020). Temporal Signatures of Criticality in Human Cortical Excitability as Probed by Early Somatosensory Responses. *The Journal of Neuroscience*, *40*, 6572–6583.

Tadel, F., Baillet, S., Mosher, J. C., Pantazis, D., & Leahy, R. M. (2011). Brainstorm: a user-friendly application for MEG/EEG analysis. *Computational intelligence and neuroscience*, *2011*, 879716.

Waschke, L., Kloosterman, N. A., Obleser, J., & Garrett, D. D. (2021). Behavior needs neural variability. *Neuron*, *172*, 341.

Waterstraat, G., Fedele, T., Burghoff, M., Scheer, H.-J., & Curio, G. (2015). Recording human cortical population spikes non-invasively--An EEG tutorial. *Journal of neuroscience methods*, *250*, 74–84.

Wikström, H., Huttunen, J., Korvenoja, A., Virtanen, J., Salonen, O., Aronen, H., & Ilmoniemi, R. J. (1996). Effects of interstimulus interval on somatosensory evoked magnetic fields (SEFs): A hypothesis concerning SEF generation at the primary sensorimotor cortex. *Electroencephalography and Clinical Neurophysiology/Evoked Potentials Section*, *100*, 479–487.